Proceedings of the Twenty-eighth (2018) International Ocean and Polar Engineering Conference **www.isope.org**
Sapporo, Japan, June 10-15, 2018

ISBN 978-1-880653-87-6; ISSN 1098-6189

Numerical Simulations of Flows around Floating Offshore Wind Turbine

Ping Cheng[1], Decheng Wan[1], Changhong Hu[2]*
[1]Collaborative Innovation Center for Advanced Ship and Deep-Sea Exploration, State Key Laboratory of Ocean Engineering, School of Naval Architecture, Ocean and Civil Engineering, Shanghai Jiao Tong University, Shanghai, China
[2]Research Institute for Applied Mechanics, Kyushu University, Fukuoka, Japan
*Corresponding Author

ABSTRACT

The fully-coupled aero-hydrodynamic simulations of a floating offshore wind turbine consisting of a NREL-5MW baseline wind turbine and a semi-submersible floating platform are conducted. The three-dimensional Reynolds Averaged Navier-Stokes (RANS) equations are solved for the coupled aero-hydrodynamic numerical simulation. The in-house code naoe-FOAM-SJTU, which is based on OpenFOAM and overset grid technology and developed for ship and ocean engineering, is employed. Aerodynamic loads on wind turbine are predicted. With the directly viscous simulations, detailed flow information around the turbine blades is available. The coupling effect on the aerodynamics of wind turbine from the platform motion is investigated.

KEY WORDS: Fully-coupled aero-hydrodynamic simulation; floating offshore wind turbine (FOWT); overset grid technology; naoe-FOAM -SJTU solver

INTRODUCTION

Floating offshore wind turbine (FOWT) has become more attractive as a type of wind energy absorption device in recent years. Due to the additional motion induced by supporting platform, the aerodynamics of the turbine blades turns more complex and unsteady. Accurate prediction of aerodynamic loads and performance of FOWT with coupling effect of floating platform motion becomes one common challenge in the designing of FOWT.

Aerodynamic performance of wind turbine operating in uniform inflow wind condition has been well researched. However, the aerodynamics of a FOWT is much more complicated. Tower shadow effects (Dolan, 2006) and shear wind effect (Thiringer, 2001) both lead to periodical oscillations on aerodynamic forces of wind turbine and asymmetry of the wake flow. And the motion of the floating support platform also induces variation of aerodynamics with motion period (Tran, 2016; Vaal, 2014). To accurately predict the aerodynamics of a floating offshore wind turbine, the fully coupled aero-hydrodynamic simulations should be conducted instead of simplified models.

To meet the technique requirement for FOWT design, fully coupled aero-hydrodynamic simulation solvers for FOWTs have been developed. In earlier studies, most numerical tools for coupling simulation of FOWT are developed based on blade element momentum (BEM) method for aerodynamic simulation and potential flow theory for hydrodynamic computation (Cordle, 2010). As BEM is an empirical method, these solvers achieve quite efficiency computations. However, some researchers (Sebastian, 2013) suggested that the BEM is still questionable in unsteady aerodynamic prediction for FOWTS with various correction models (such as Glauert correction, skewed wake correction, etc.). Additionally, the hydrodynamic simulation based on potential flow theory restricts the usage for more accurate predictions with the viscous effect. With rapid development of compute technology and computing methods, fully coupled studies have been conducted with CFD method are conducted. Tran (2015) has conducted the fully coupled aero-hydrodynamic analysis of a semi-submersible FOWT using a dynamic fluid body interaction approach with Star CCM+ software combined with overset grid technique. Based on OpenFOAM package, Liu (2017) established a fully coupled CFD analysis tool for FOWTs and studied the coupling effect of the OC4 DeepCWind semi-submersible FOWT.

With fully coupled aero-hydrodynamic simulation of a FOWT, this paper mainly pay attention to the analysis of the coupling effect between the aerodynamics of turbine blades and the hydrodynamic motions of the supporting platform. The fully-coupled aero-hydrodynamic simulations of a floating offshore wind turbine consisting of the NREL-5MW baseline wind turbine and a semi-submersible floating platform are conducted. The three-dimensional Reynolds Averaged Navier-Stokes (RANS) equations are solved for the coupled aero-hydrodynamic numerical simulation. The in-house code naoe-FOAM-SJTU is employed, which is based on OpenFOAM and overset grid technology and developed for ship and ocean engineering. The aerodynamic (Cheng, 2016) and hydrodynamic (Cheng, 2015) validations of naoe-FOAM-SJTU are done in our previous work, which show the reliability of this solver. With directly viscous simulations, detailed flow information around the turbine blades is available. The coupling effect on the aerodynamics of wind turbine from the platform motion is investigated.

NUMERICAL METHOD

naoe-FOAM-SJTU Solver

Based on the open source CFD platform, the in-house code naoe-FOAM-SJTU solver (Cao, 2014) is designed for computing viscous flows of ships and ocean structures. It inherits the data structure and CFD libraries in OpenFOAM, such as FVM, RANS, VOF and PISO algorithm. The two-phase incompressible RANS equations are solved in this solver. The governing equations are discretized with Finite Volume Method (FVM) which is capable to handle arbitrary polyhedral cells. The interface between two phases is captured using a VOF method with bounded compression technique. The turbulence models of k–ω SST and k−ε can be used for turbulence closure. The pressure-velocity coupling equations are solved by Pressure-Implicit with Splitting of Operations (PISO) algorithm. Based on the above, a numerical tank system including wave generation and absorption module is built up, six-degree-of-freedom (6DOF) motion module is developed, and finally the mooring system module is established (Fig.1).

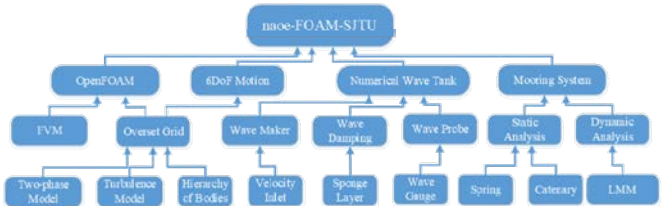

Fig.1 Frame Diagram of naoe-FOAM-SJTU Solver

The wave generation system is able to use inlet boundary to generate first order regular waves and higher order nonlinear waves, transient extreme waves and even freak waves. The sponge layer for wave absorption is adopted to avoid wave reflection. The mooring system module is built for hydrodynamic analysis of floating offshore structures which are moored in waters, such as Semi-submersible, TLP, Spar and FPSO. Several quasi static models including spring, catenary, piecewise extrapolation method as well as a dynamic model lumped mass method, are utilized for simulation of mooring lines. To solve 6DOF equations, two coordinate systems are used, which are the earth-fixed coordinate system and the body-fixed coordinate system. And both dynamic deformation mesh method and overset grid technique are employed to deal with the 6DOF issues. With these modules, naoe-FOAM-SJTU solver can be applied to the simulation of ship advancing, sea-keeping, superposition of complex motions, and hydrodynamics of floating platforms.

Governing Equations

In the numerical simulations in this paper, the incompressible Reynolds-Average Navier-Stokes (RANS) equations are solved, which contain the continuity equations and the momentum equations:

$$\frac{\partial U_i}{\partial x_i} = 0 \tag{1}$$

$$\frac{\partial U_i}{\partial t} + \frac{\partial}{\partial x_j}(U_i U_j) = -\frac{1}{\rho}\frac{\partial P}{\partial x_i} + \frac{\partial}{\partial x_j}\left(\nu \frac{\partial U_i}{\partial x_j} - \overline{u_i' u_j'}\right) \tag{2}$$

In these equations, U_i represents the averaged flow velocity component, while u_i' is the fluctuation part; ρ is the density of the fluid; P is the pressure; ν is the kinematic viscosity.

But the equations are not closed as they contain more variables than there are equations. In order to meet the closure requirement and solve the above equations, the two-equation turbulence model k-ω SST (Menter, 1994) is employed, and the turbulent kinetic energy k and the turbulent dissipation rate ω can be described as:

$$\frac{\partial}{\partial t}(\rho k) + \frac{\partial}{\partial x_i}(\rho k u_i) = \frac{\partial}{\partial x_j}\left(\Gamma_k \frac{\partial k}{\partial x_j}\right) + G_k - Y_k + S_k \tag{3}$$

$$\frac{\partial}{\partial t}(\rho \omega) + \frac{\partial}{\partial x_i}(\rho \omega u_i) = \frac{\partial}{\partial x_j}\left(\Gamma_\omega \frac{\partial \omega}{\partial x_j}\right) + G_\omega - Y_\omega + D_\omega + S_\omega \tag{4}$$

In the above equations, Γ_k and Γ_ω are the effective diffusion coefficients, G_k and G_ω are turbulence generation terms, Y_k and Y_ω are turbulent dissipation terms, S_k and S_ω are the source term, D_ω is the cross-diffusion term for ω.

Overset Grid Technique

Using overset grid technique, the separated overlapping grids for each part with independent movement are allowed, which makes it powerful in simulating large amplitude motion problems. And the information transformation between each grid domain is built by interpolation at appropriate cells or points using DCI (domain connectivity information) which is produced by SUGGAR++ (Carrica, 2010). There are four main steps when using DCI in the overset grid technique: The first step is to pick out the hole cells which are located outside the simulation domain or of no interest, and exclude them from computation. As shown in Fig.2, in overset grid, there exist series of fringe cells around hole cells, and for each fringe cell there are several donor cells which receive information from the donor cells, so the next step is to search the donor cells of each fringe cell and provide information from the donor grids. The third step is to obtain the value of a variable ϕ of the fringe cell by interpolation from the donor cells with:

$$\phi_I = \sum_{i=1}^{n} \omega_i \cdot \phi_i, \qquad \sum_{i=1}^{n} \omega_i = 1 \tag{5}$$

Where ϕ_I is the value of a variable ϕ of the fringe cell, ϕ_i is the value for the i^{th} donor cell, ω_i is the dimensionless weight coefficient.

And the last step is to optimize the overlapping area and improve the accuracy of interpolation.

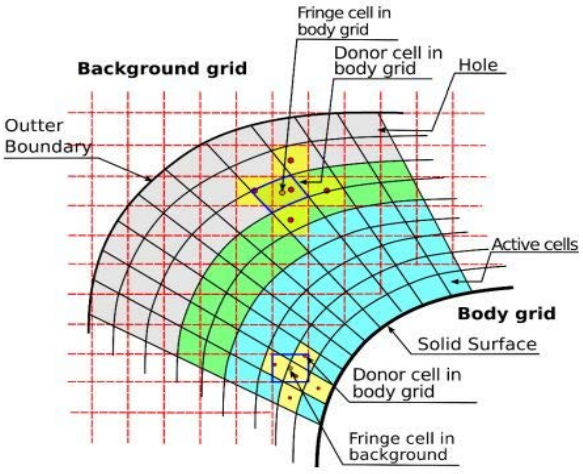

Fig.2 Diagram of Overset Grid

GEOMETRY MODEL

The semi-submersible floating offshore wind turbine

In the present simulation work, a semi-submersible floating offshore wind turbine (FOWT) system, Phase II of OC4 project, is adopted. The FOWT contains several main parts: a wind turbine (the NREL 5-MW baseline wind turbine (Jonkman, 2009)), a tower connecting wind turbine and platform, a supporting floating platform (semi-submersible platform (Robertson, 2012)), and the mooring system. Fig.3 shows the sketch of this FOWT system, and Table.1 lists the basic properties.

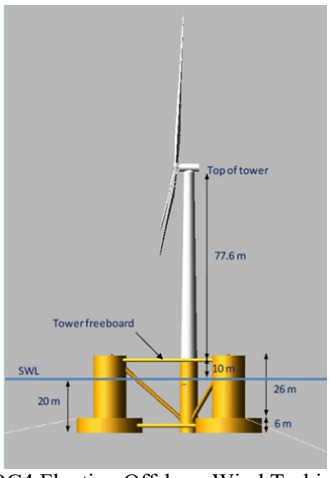

Fig.3 Phase II of OC4 Floating Offshore Wind Turbine System

Table.1 Specification of the Phase II of OC4 FOWT System

Rotor Orientation, Configuration	Upwind, 3 Blades
Rotor, Hub Diameter	126 m, 3 m
Hub Height	90 m
Rotor Mass	110,000 kg
Nacelle Mass	240,000 kg
Tower Mass	347,460 kg
Coordinate Location of CM (rotor, nacelle and tower)	(-0.2 m, 0.0 m, 64.0 m)
Total draft of platform	20m
Platform Mass	1.347E7 kg
Coordinate Location of CM (platform)	(0.0 m, 0.0 m, -13.46 m)
Number of Mooring Lines	3
Angle Between Adjacent Lines	120°
Depth to Anchors/Fairleads Below SWL	200m, 14m
Radius to Anchors/Fairleads from Platform Centerline	837.6m, 40.868m
Unstretched Mooring Line Length	835.5m
Mooring Line Diameter	0.0766m
Equivalent Extensional Stiffness	7.536E+8N
Equivalent Mass Density/ in water	113.35kg/m, 108.63kg/m

Table.2 Structural Properties of the FOWT System

Structural mass	1.407E7kg
CM location below SWL	9.9376m
Total structure roll inertia about CM	1.1E10 kg*m^2
Total structure pitch inertia about CM	1.1E10 kg*m^2
Total structure yaw inertia about CM	1.226E10 kg*m^2

The wind turbine in Phase II of OC4 FOWT system is NERL 5-MW baseline line wind turbine, which is a conventional three-bladed, upwind, variable-speed wind turbine. The floating support platform is a semi-submersible floating system which consists of a main column attached to the tower, three offset columns covering significant portion of buoyancy, a couple of smaller diameter pontoons and cross braces to link the main column and offset columns and to strengthen the structure. The semi-submersible floating system for Phase Ⅱ of OC4 is moored with three catenary lines spread symmetrically about the platform Z-axis.

Setup of Simulation Domain

The optimum domain should be large enough to avoid boundary effects. Since the numerical simulations are conducted under the regular wave with wave length of 156.13m, the domain is set as cuboid with X (-200m~400m), Y (-150m~150m), Z (-100m~240m), as shown in Fig.4. As the overset grid technique is utilized, three grid systems are generated respectively. The green color in Fig4 represents for the background mesh covering the whole simulation domain, which is refined along the wave surface to reach grid density requirement for surface capture and also refined near the other two mesh system for better interpolation. The yellow cylinder sub-domain contains the wind turbine including turbine blades, nacelle and hub. In this paper, all the solid structures are treated as rigid body, so the red part of grid is generated with the platform and tower.

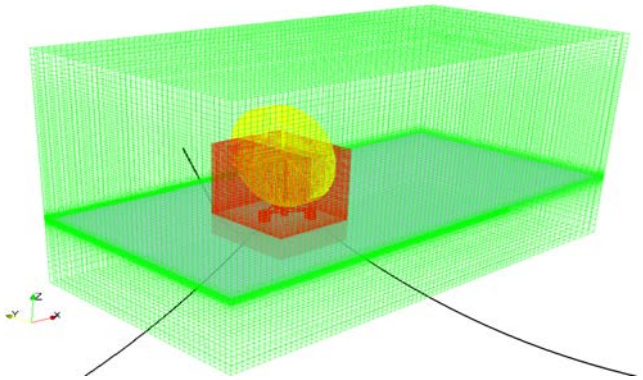

Fig.4 Simulation Domain

RERULTS AND DISCUSSIONS

In the present work, the fully coupled aero-hydrodynamics of a FOWT in coupling wave-wind conditions are investigated. The FOWT operate in regular heading wave with wave height of 4m and wave length of 156.13m, coupled with constant 8m/s inflow wind in which case the turbine rotating speed is a fixed value of 9.2rpm. The coupling effect between the hydrodynamic motions of floating wind turbine and the aerodynamic loads on wind turbine makes the dynamic performance of FOWT quite complicated.

Dynamic motions of floating platform

The main difference between a floating offshore wind turbine and a conventional floating platform is the existence of the wind turbine. In regular heading waves, a moored bare platform with symmetrically distributed mooring lines oscillates with wave period in three main degrees of freedom (DOFs): surge, heave and pitch, while the motions in other DOFs are negligible. This oscillations result from the periodic wave loads on the floating platform, and the equilibrium position for oscillating motions are determined where the total forces of mooring

lines counterbalances the quadratic composition of hydrodynamic forces. But for a FOWT, the rotating wind turbine provides an additional thrust. This thrust is negligible compared to the periodic hydrodynamic wave forces on the platform. However it is too large to be neglected compared with the averaged mooring forces in the initial equilibrium position. So the equilibrium position moves forward to find a new force balancing situation.

The surge curve in Fig.5 (a) shows an sinusoidal motion with equilibrium position located around X=8.9m, which is no more than 2m away from the initial center of mooring system in bare platform cases. This oscillating motion of floating platform is transferred to turbine blades through the tower, which results in the variation of the relative velocity near turbine blades.

The rotating turbine rotor acts as an appendage part of the whole floating offshore wind turbine. So the additional pitching moment from aerodynamics of turbine blades is computed by integral the moments on each blade surface cell to the rotating center. As the time history of pitch motion shown in Fig.5 (b), this additional pitching moment plays a similar role in the pitching motion just as the additional thrust force does in surging motion DOF. Similar conclusions are drawn for the pitching motion. However, it's worth noting that the phase difference between pitch motion and surge motion is around 180deg.

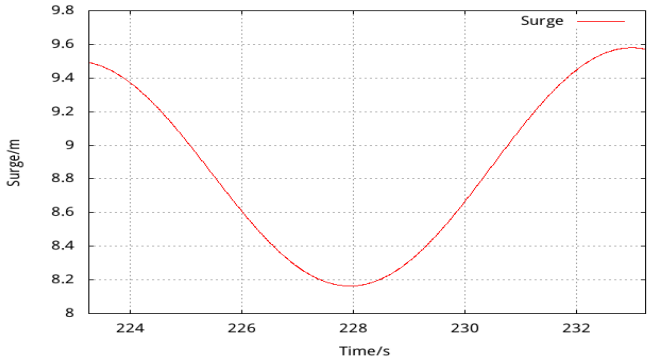

(a) Dynamic surge motion

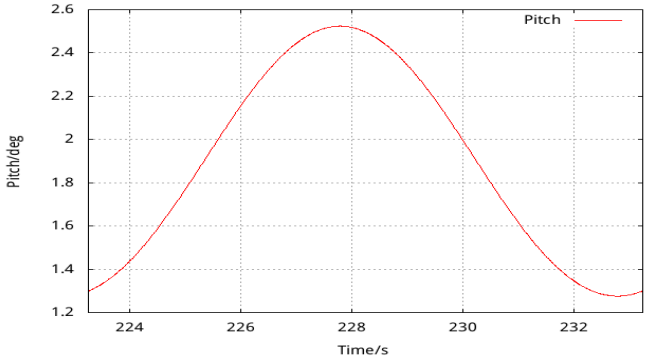

(b) Dynamic pitch motion

Fig.5 Dynamic motions of floating platform during one wave period

Aerodynamic forces on wind turbine

A bottom-fixed wind turbine rotating in uniform wind is supposed to be subject to periodically varying aerodynamic forces considering the tower effect. The period of the varying forces is 1/3 of the rotating period for this 3-bladed wind turbine. In this simulation, the rotational period is 6.52s, so about 4.5 cycles of varying thrust during one wave period is indicated in Fig.6. The minimum value is captured when one blade rotating to the right upstream of the tower.

The wind turbine mounted on the floating platform operates with an additional motion transferred from the support platform, which is described in the last paragraph. The additional motion speed caused by platform surge is in the range of -0.45m/s~0.45m/s on the whole turbine structure. Nevertheless, the additional velocity on blades surface resulting from pitch motion round the rotating center lying 10m below the still water surface linearly varies with the distance to the rotating center, which is calculated by multiplying the pitching angular velocity and the distance from the calculated cell to the rotating center. The range of angular speed is -0.42deg~0.42deg, the distance range of turbine blades is 37m~163m, so the additional velocity caused by pitch motion on top of rotor varies within range of -1.19m/s~1.19m/s, while the lowest point in the rotating plane varies within: -0.27m/s~0.27m/s. What is noticeable is that the phase difference between surge and pitch has reached 180deg, in which case surge and pitch motion have opposite effects on the additional velocity of turbine structure. So fortunately, coupling these two key factors doesn't result in significant variation on the aerodynamic thrust but offsets it to a certain extent.

The time history of aerodynamic thrust is plotted in Fig.6. The aerodynamic thrust curve show oscillating regularity with wave period. During 223s~228s, turbine blades pitches towards downstream while surges towards -x direction, the additional motion induced with surge has the positive effect to increase the relative flow speed and the pitch motion has the negative effect. Nevertheless, the aerodynamic thrust during this half period is lower than the average value, which illustrate that the pitch motion plays the dominant role in this operating condition. In the following half period during 228s~233s, the aerodynamic thrust during decrease below the average value while turbine blades moves in the opposite direction.

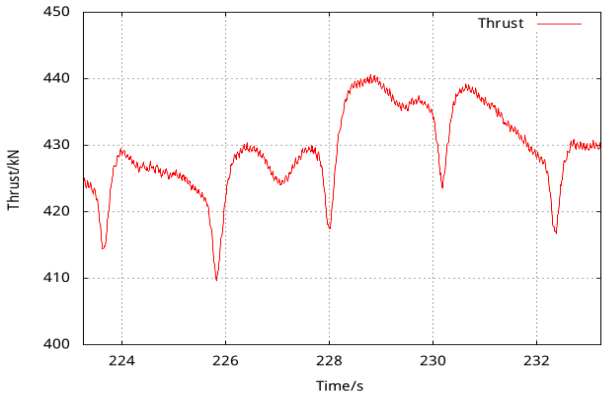

Fig.6 Aerodynamic thrust on wind turbine during one wave period

Wake flow field

Flow field around wind turbine is disturbed by the rotating turbine blades. Initial flow velocity drives the disturbed flow moving downstream with interaction with the undisturbed flow. For a rotor-fixed wind turbine rotating with fixed speed in uniform wind field, the wake flow should be helical symmetry. However, the wake flow for a FOWT is much more complicated due to the non-uniform wind, the tower effect, and the additional motion aligned to the floating platform.

Fig.7-9 show the flow velocity distributions during one wave period in the longitudinal section, and Fig.10-12 show the flow velocity distributions in a tilted transverse section which overlaps with the rotating plane of turbine blades at equilibrium pitching position. The flow field is colored with value of velocity component, the platform surface is colored with pressure value, and the interface between air and wave is visualized with a blue line. The pressure on the platform surface increases rapidly with water depth as illustrated in those figures. Velocity distribution of flow velocity component U_x indicates that the

flow velocity decreases significantly while passing through the turbine rotating plane. It is also noticed that the velocity decrease is more prominent behind the tower. Even on the cross section about 5m ahead of tower, the variation of flow velocity is also captured as a green vertical band region in Fig.10. The tower effect is also noticed in the U_y component in Fig.11 with a light blue band on right side and a light orange band on left side below the rotor center.

The U_y and U_z components for inflow wind are both set as zero, but the rotating turbine blades induce the U_y and U_z of surrounding flow significantly. As the velocity increases from turbine center to blade tip, the induced flow velocity grows rapidly as illustrated in Fig.11-12. The Fig.10-12 the +y direction points from right to left, and the wind turbine rotates in clockwise direction, so the value of induced U_y component is supposed to be negative at in the flow field above the rotor center, and be positive in the below region. However, besides the dark blue regions, there are also red and orange regions which represent positive U_y value. This confusion can be explained with the U_y distribution in Fig.13-14, which shows the flow velocity distribution surrounding the blade in section#1 and section#2. Section#1 and section#2 are located on the same blade with different distance to the rotor center as shown in the third figure in Fig.12. Because of the asymmetry of the airfoil, when the airfoil rotates through flow, the velocity distribution becomes asymmetric. And the induced velocity on the downstream side is positive, while flow velocity near leading edge and trailing edge is negative. The initial value of velocity component U_z is also set as zero in the whole flow field, so similar regularities are got.

Because the flow velocity component U_y and U_z are induced with the rotating motion of turbine blades, so the magnitude of induced velocity increases rapidly with towards the blades tip. While the most significant motions aligned with platform, which is surge and pitch in this simulation, mainly affects the relative velocity component U_x. As discussed above, the pitch motion plays the predominant role in the motion of blades section. In the first figure and the last figure in Fig.7 when turbine surge back in –X direction and pitch forward along +x direction, velocity increase is observed in the flow field near the downstream surface of the top blade and the value gets larger as height grows.

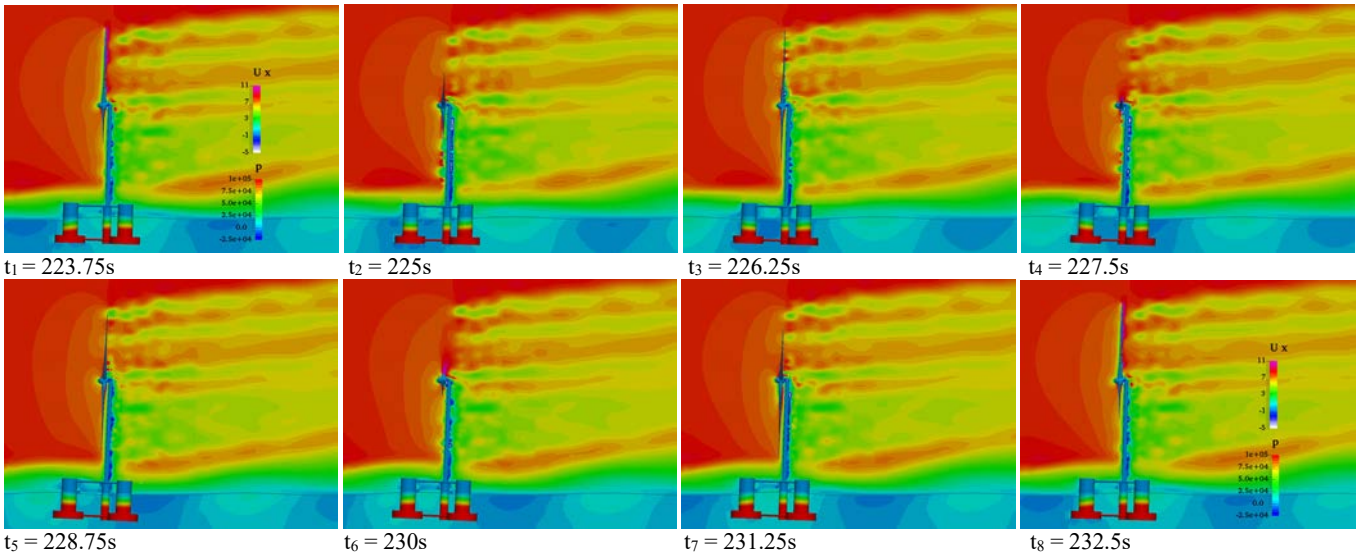

Fig.7 Distribution of the flow velocity component U_x on a longitudinal section across turbine center during one wave period

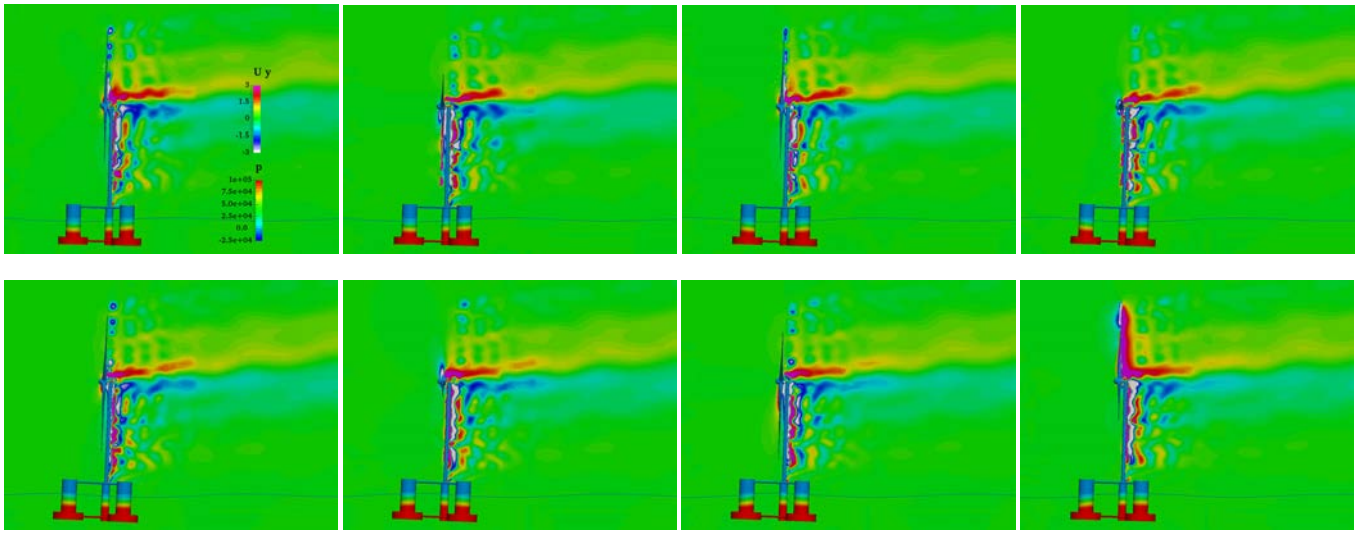

Fig.8 Distribution of the flow velocity component U_y on a longitudinal section across turbine center during one wave period

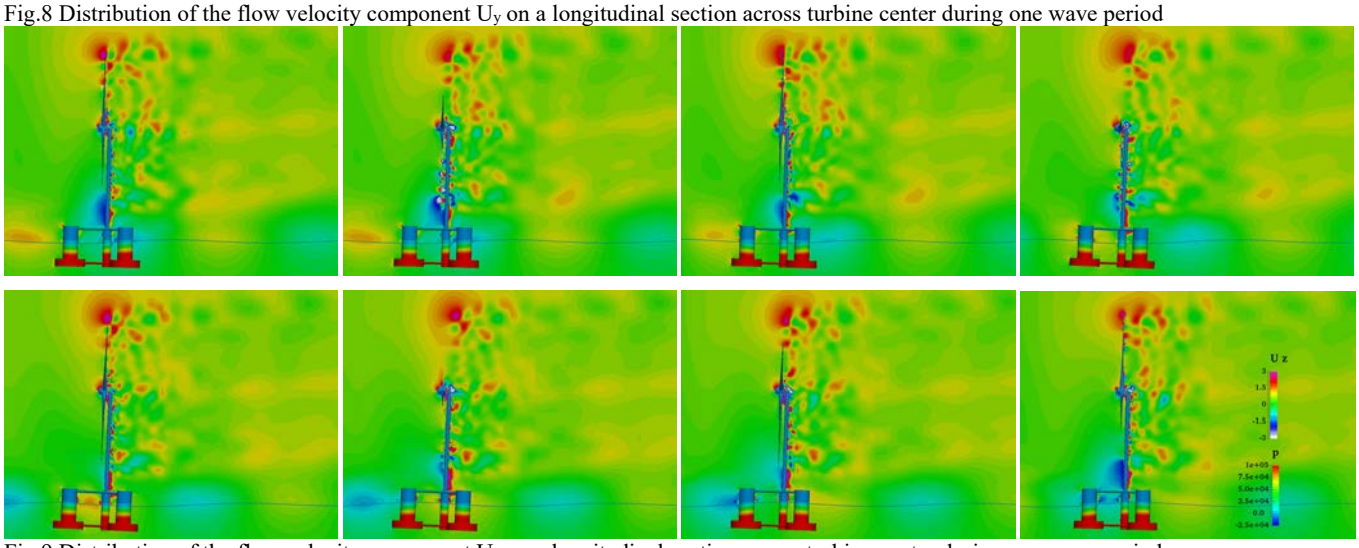

Fig.9 Distribution of the flow velocity component U_z on a longitudinal section across turbine center during one wave period

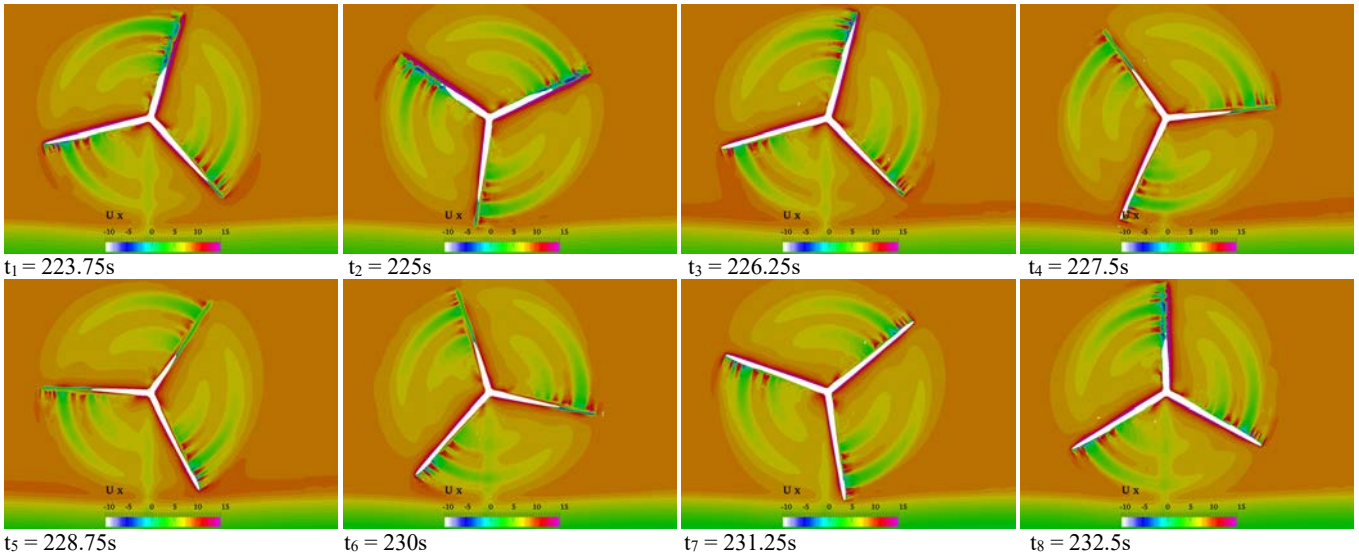

t_1 = 223.75s t_2 = 225s t_3 = 226.25s t_4 = 227.5s

t_5 = 228.75s t_6 = 230s t_7 = 231.25s t_8 = 232.5s

Fig.10 Distribution of the flow velocity component U_x on a cross section across turbine center during one wave period

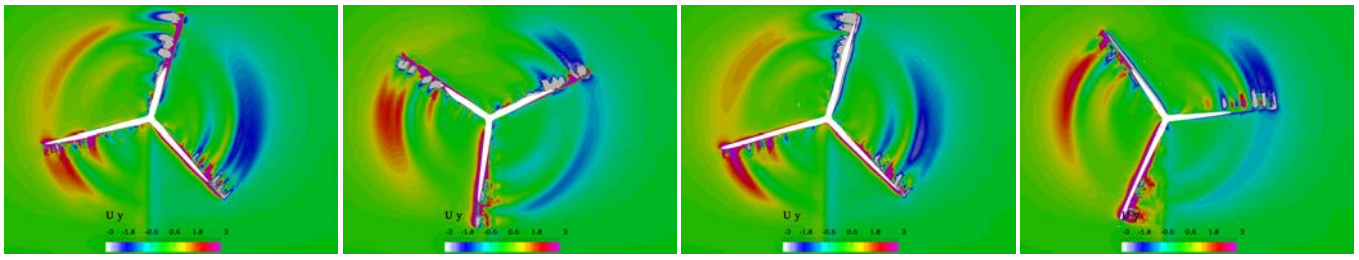

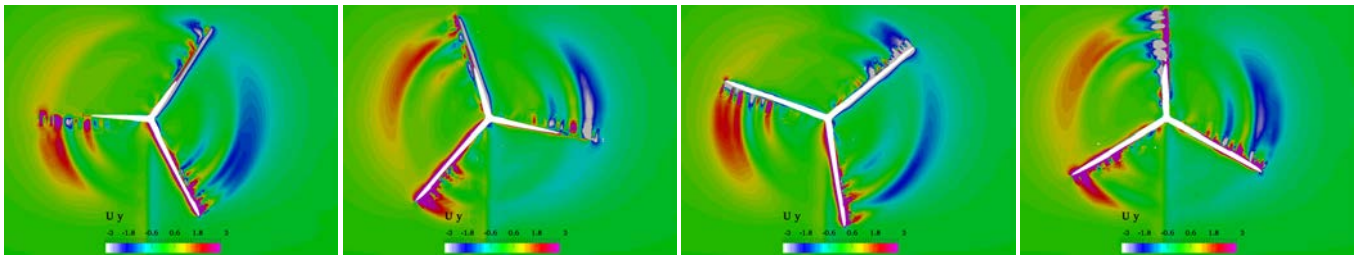

Fig.11 Distribution of the flow velocity component U_y on a cross section across turbine center during one wave period

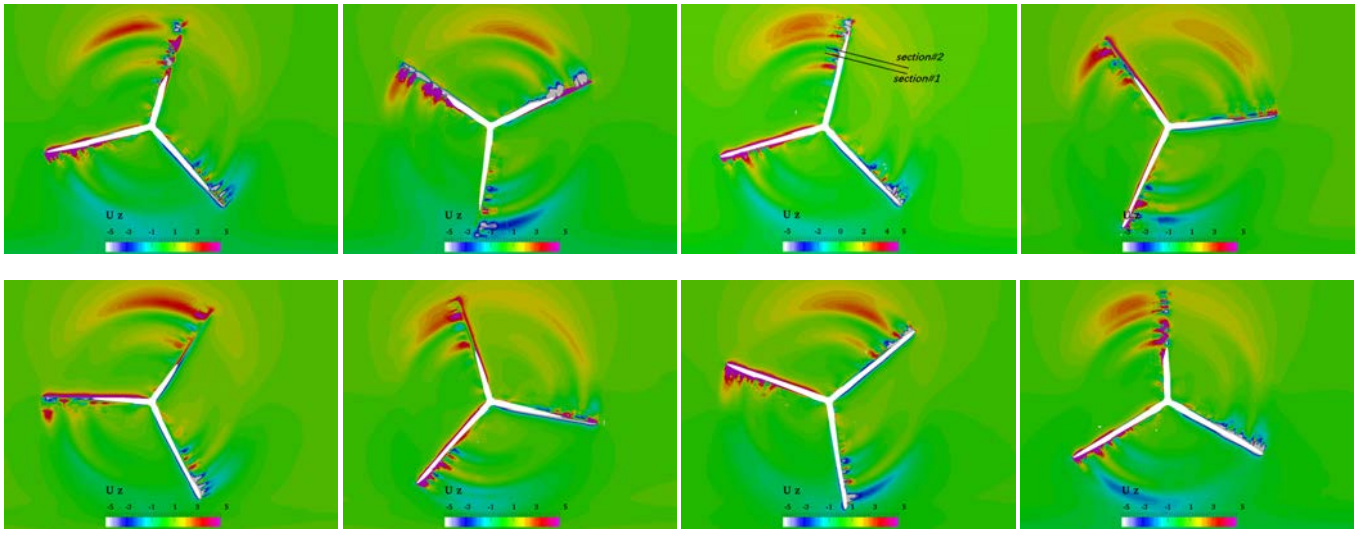

Fig.12 Distribution of the flow velocity component U_z on a cross section across turbine center during one wave period

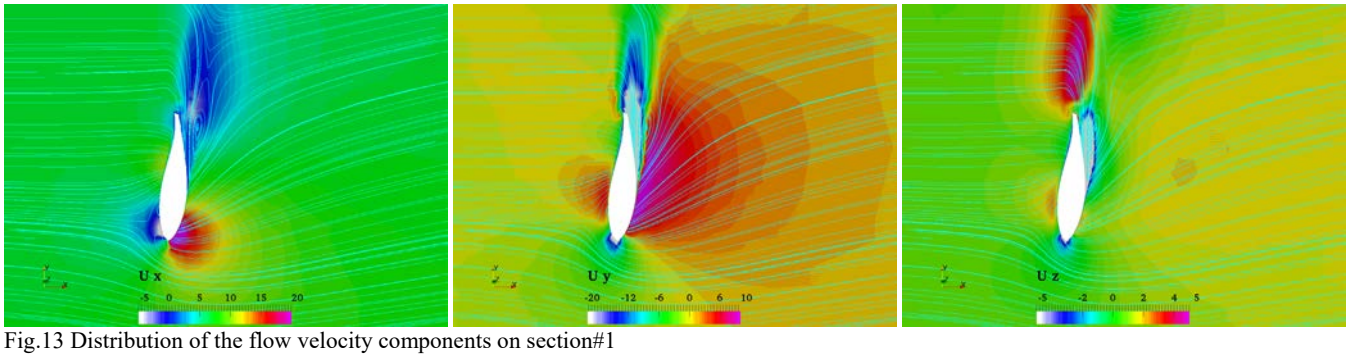

Fig.13 Distribution of the flow velocity components on section#1

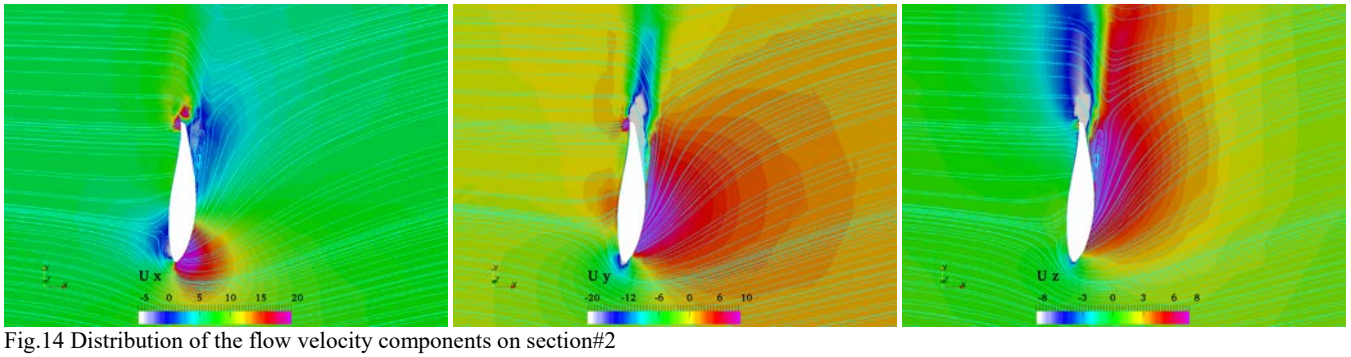

Fig.14 Distribution of the flow velocity components on section#2

CONCLUSIONS

The fully-coupled aero-hydrodynamic simulation of NREL-5MW baseline wind turbine mounted on a semi-submersible floating platform is conducted. The in-house code naoe-FOAM-SJTU solver, based on OpenFOAM and coupled with overset grid technology, is employed. The three-dimensional Reynolds Averaged Navier-Stokes (RANS) equations are solved, coupling with the k-ω SST turbulence model.

The additional aerodynamic forces on turbine blades mainly affect the equilibrium position of the FOWT system in surge and pitch DOFs. Both periodic surge and pitch motions of blades in sync with platform results in the variations of the relative flow velocity nearby blades surface. But the phase difference between the motions is almost 180deg, in which case surge and pitch motion have opposite effects on the additional velocity of turbine structure. So coupling these two key factors doesn't result in significant variation on the aerodynamic thrust but offsets it to a certain extent. And in this simulation case, the pitch motion effect plays the predominant role. Detailed flow information also clarifies the flow filed and indicates the coupling effects. The rotating motion of rotor blades induces rotational velocity of surrounding flow. The additional surge and pitch motion aligned with platform mainly affects the relative velocity component U_x in the surrounding flow field. The tower effect and the additional motions make the wake flow field more complicated.

ACKNOWLEDGEMENTS

This work is supported by the National Natural Science Foundation of China (51490675, 11432009, 51579145), Chang Jiang Scholars Program (T2014099), Shanghai Excellent Academic Leaders Program (17XD1402300), Program for Professor of Special Appointment (Eastern Scholar) at Shanghai Institutions of Higher Learning (2013022), Innovative Special Project of Numerical Tank of Ministry of Industry and Information Technology of China (2016-23/09) and Lloyd's Register Foundation for doctoral student, to which the authors are most grateful.

REFERENCES

Cao, HJ, Wan, DC. (2014). Development of Multidirectional Nonlinear Numerical Wave Tank by naoe-FOAM-SJTU Solver, International Journal of Ocean System Engineering, Vol. 4, No. 1, pp. 52-59.

Carrica, PM, Huang, J, Noack R. (2010). Large-scale DES computations of the forward speed diffraction and pitch and heave problems for a surface combatant [J]. Computers & Fluids, 39(7): 1095-1111.

Cheng, P, Wan, DC. (2015). Hydrodynamic analysis of the semi-submersible floating wind system for phase II of OC4[C]. The Twenty-fifth International Ocean and Polar Engineering Conference. Kona, Hawaii, USA.

Cheng, P, Ai, Y, Wan, DC. (2016). Unsteady Aerodynamic Simulations of Floating Offshore Wind Turbines with Coupled Periodic Surge and Pitch motions[C]. In the 12th International Conference on Hydrodynamics. Egmond aan Zee, The Netherlands.

Cordle, A. (2010). State-of-the-art in design tools for floating offshore wind turbines. Deliverable Report Under (SES6), UpWind project, Bristol, UK, Contract.

Dolan, D. S., & Lehn, P. W. (2006). Simulation model of wind turbine 3p torque oscillations due to wind shear and tower shadow. IEEE Transactions on energy conversion, 21(3), 717-724.

Jonkman, J, Butterfield, S, Musial, W, Scott, G (2009). Definition of a 5-MW reference wind turbine for offshore system development. Golden, CO: National Renewable Energy Laboratory.

Liu, YC, Xiao, Q, Incecik, A, Incecik, A, Peyrard, C, Wan DC. (2017). Establishing a fully coupled CFD analysis tool for floating offshore wind turbines. Renewable Energy, 112: 280-301.

Menter, FR. (1994). Two-equation eddy-viscosity turbulence models for engineering applications. AIAA journal, 32(8): 1598-1605.

Quallen, S, Xing, T, Carrica, P, Li, Y, Xu, J. (2013). CFD simulation of a floating offshore wind turbine system using a quasi-static crowfoot mooring-line model. In The Twenty-third International Offshore and Polar Engineering Conference. Alaska, USA.

Robertson, A, Jonkman, J, Masciola, M. (2012). Definition of the Semisubmersible Floating System for Phase II of OC4. Offshore Code Comparison Collaboration Continuation (OC4) for IEA Task, 30.

Sebastian, T, Lackner, MA. (2013). Characterization of the unsteady aerodynamics of offshore floating wind turbines. Wind Energy, 16(3): 339-352.

Thiringer, T, Dahlberg, J. A. (2001). Periodic pulsations from a three-bladed wind turbine[J]. IEEE Transactions on Energy Conversion, 16(2): 128-133.

Tran, T T, Dong, HK. (2015). The aerodynamic interference effects of a floating offshore wind turbine experiencing platform pitching and yawing motions. Indian Journal of Thoracic and Cardiovascular Surgery, 29 (2): 549–561.

Tran, T. T., & Kim, D. H. (2016). A CFD study into the influence of unsteady aerodynamic interference on wind turbine surge motion. Renewable Energy, 90, 204-228.

Vaal, J. D., Hansen, MO, Moan, T. (2014). Effect of wind turbine surge motion on rotor thrust and induced velocity. Wind Energy, 17(1), 105-121.